Research Square

Preprints are preliminary reports that have not undergone peer review.
They should not be considered conclusive, used to inform clinical practice,
or referenced by the media as validated information.

Donor-Level Public-Data Analysis of Proteostasis–Translation–Metabolism Coupling in Cardiomyocytes From Patients With Heart Failure With Preserved Ejection Fraction

Yufeng He
Department of Cardiology, The Affiliated Hospital of Southwest Medical University, Luzhou, Sichuan, 646000, China;

Hu Tan
Department of Respiratory and Critical Care Medicine, The Affiliated Hospital of Southwest Medical University, Luzhou, Sichuan, 646000, China;

Rui Pu
Department of Endocrinology and Metabolism, The Affiliated Hospital of Southwest Medical University, Luzhou, Sichuan, 646000, China;

Jialin Ma
Institute of Stomatology, Southwest Medical University, Luzhou, Sichuan, 646000, China.

Hanxi Zhang
Institute of Stomatology, Southwest Medical University, Luzhou, Sichuan, 646000, China.

Chunxiang Zhang
zhangchunxiangKZL@163.com

Department of Cardiology, The Affiliated Hospital of Southwest Medical University, Luzhou, Sichuan, 646000, China;

Xiaorong Lan
Institute of Stomatology, Southwest Medical University, Luzhou, Sichuan, 646000, China.

Research Article

Keywords: HFpEF, cardiomyocytes, single-nucleus RNA sequencing, proteostasis, translation, oxidative phosphorylation, systems immunology, public-data integration

Posted Date: November 11th, 2026

DOI: https://doi.org/10.21203/rs.3.rs-11491507/v1

License: This work is licensed under a Creative Commons Attribution 4.0 International License.
Read Full License

Additional Declarations: No competing interests reported.

Donor-Level Public-Data Analysis of Proteostasis–Translation–Metabolism Coupling in Cardiomyocytes From Patients With Heart Failure With Preserved Ejection Fraction

Yufeng He[1,2], Hu Tan[3], Rui Pu[4], Jialin Ma[5,6], Hanxi Zhang[5,6], Chunxiang Zhang[1,2*],Xiaorong Lan[5,6*]

1 Department of Cardiology, The Affiliated Hospital of Southwest Medical University, Luzhou, Sichuan, 646000, China;

2 Nucleic Acid Medicine of Luzhou Key Laboratory, Southwest Medical University, Luzhou , Sichuan, 646000, China;

3 Department of Respiratory and Critical Care Medicine, The Affiliated Hospital of Southwest Medical University, Luzhou, Sichuan, 646000, China;

4 Department of Endocrinology and Metabolism, The Affiliated Hospital of Southwest Medical University, Luzhou, Sichuan, 646000, China;

5 Institute of Stomatology, Southwest Medical University, Luzhou, Sichuan, 646000, China.

6 Luzhou Key Laboratory of Oral & Maxillofacial Reconstruction and Regeneration, The Affiliated Stomatological Hospital, Southwest Medical University, Luzhou, Sichuan, 646000, China;

Yufeng He, Hu Tan and Rui Pu contributed equally to this work.

*Corresponding author: Chunxiang Zhang, E-mail: zhangchunxiangKZL@163.com, Xiaorong Lan, E-mail: xiaoronglancdm@163.com

Abstract

Heart failure with preserved ejection fraction (HFpEF) is biologically heterogeneous, and the relationship between myocardial metabolic stress, proteostasis, and immune composition remains incompletely defined. We established a prespecified proteostasis–translation–metabolism coupling-failure (PTM-CF) framework and evaluated it using public human and mouse datasets. The primary analysis used the complete authorized H5AD CellBender raw-count layer from the human SCP3342 single-nucleus dataset and treated donors rather than nuclei as biological replicates. The discovery

set comprised 14,644 cardiomyocyte nuclei from 43 donors, including 19 HFpEF donors and 24 non-failing controls. Donor-level pseudobulk models were adjusted for sex and biosample/pool. Translation-load index (TLI), proteostasis-capacity index (PCI), metabolic-supply index (MSI), and a prespecified PTM-CF composite were calculated from frozen gene modules. TLI was lower in HFpEF cardiomyocytes (β = −0.260, 95% CI −0.419 to −0.100, FDR = 0.00460), as was MSI (β = −0.233, 95% CI −0.320 to −0.147, FDR = 1.65 × 10−5). PCI was directionally lower but not significant (β = −0.0635, 95% CI −0.190 to 0.0628, FDR = 0.314). The PTM-CF composite was higher in the discovery model (β = 0.953, 95% CI 0.123 to 1.783, FDR = 0.0342), requiring independent replication. A prespecified immune-composition analysis found a higher lymphocyte fraction (β = 0.01351, FDR = 0.00382) and lower cycling-macrophage fraction (β = −0.00579, FDR = 0.000816), whereas the overall immune-labeled fraction was not different (FDR = 0.4529). A frozen 18-gene cardiomyocyte inflammatory score was not significantly higher in HFpEF (FDR = 0.6623) and was not significantly associated with PTM-CF (FDR = 0.2395). In human myocardial proteomics, 25 frozen-module genes were matched and 17/25 showed concordant RNA–protein direction, although global correlation was not significant (Spearman ρ = 0.158, P = 0.452). ACADVL and HADHA were the most convergent computational candidates across human cardiomyocyte RNA, human myocardial protein, and mouse HFpEF protein evidence. These findings support an auditable model of HFpEF metabolic, proteostasis, and immune-composition remodeling, but do not establish generalized immune activation, cytokine release, HFpEF specificity, causality, therapeutic efficacy, or target validation.

Keywords: HFpEF; cardiomyocytes; single-nucleus RNA sequencing; proteostasis; translation; oxidative phosphorylation; systems immunology; public-data integration

Introduction

Heart failure with preserved ejection fraction (HFpEF) is a heterogeneous clinical syndrome associated with metabolic disease, hypertension, obesity, inflammation, microvascular dysfunction, and myocardial remodeling [7–11]. Contemporary models emphasize the interaction of systemic comorbidities with coronary microvascular dysfunction, endothelial inflammation, myocardial fibrosis, and impaired reserve rather than a single cardiac lesion [12–14]. Cardiomyocytes must sustain continuous contractile work while maintaining protein synthesis, folding, degradation, organelle quality control, and mitochondrial energy production. Disruption at any one of these levels may alter myocardial function, yet translation, proteostasis, and metabolic supply are often analyzed separately [15–18].

We therefore developed a prespecified and auditable proteostasis–translation–metabolism coupling-failure (PTM-CF) framework. The framework does not assume that HFpEF necessarily produces a composite coupling defect. Instead, it defines three independently testable programs: a translation-load index (TLI), representing translation and ribosome-associated demand; a proteostasis-capacity index (PCI), representing protein quality-control capacity across endoplasmic-reticulum, degradation, and mitochondrial-proteostasis programs; and a metabolic-supply index (MSI), representing fatty-acid oxidation, the tricarboxylic-acid cycle, electron transport, and oxidative phosphorylation. The composite is defined as:

PTM-CF=z(TLI)−z(PCI)−z(MSI).PTM\text{-}CF = z(TLI) - z(PCI) - z(MSI).PTM-CF=z(TLI)−z(PCI)−z(MSI).

Under this definition, PTM-CF increases when translation-related demand is high relative to proteostasis capacity and metabolic supply. The composite is interpreted only together with its component indices and their directions. A significant composite without coherent component-level support is not sufficient to establish a biological coupling failure.

The study had four objectives. First, we tested TLI, PCI, MSI, and PTM-CF in donor-level cardiomyocyte data from the human SCP3342 HFpEF single-nucleus dataset. Second, we evaluated gene-level signals and RNA–protein directional concordance using human myocardial proteomics. Third, we assessed cross-species directionality using a mouse SAUNA-HFpEF proteome/phosphoproteome resource. Fourth, we added a prespecified immune-composition and cardiomyocyte inflammatory-state validation layer without modifying the frozen PTM-CF modules or using immune results to re-rank candidates.

The study was designed to distinguish discovery, orthogonal evidence, generalization, and validation. It does not claim HFpEF specificity because a compatible HFrEF/DCM donor-level comparator was unavailable. It also does not claim complete clinical adjustment, genetic causality, immune activation, therapeutic efficacy, or target validation.

Materials and Methods

Study design and data resources

This was an observational, computational, public-data integration study with a human-first, donor-level design. The discovery resource was SCP3342, a human septal endomyocardial single-nucleus RNA-sequencing dataset. Orthogonal human evidence was obtained from PRIDE/ProteomeXchange accession PXD045677, a human myocardial proteomics resource. Cross-species generalization was assessed using PRIDE accession PXD033501, a male mouse SAUNA-HFpEF proteome/phosphoproteome resource. HERMES 2024 non-ischemic HFpEF GWAS data were retained as a genetics-prioritization anchor, but colocalization, TWAS, and Mendelian-randomization analyses were not run because complete lawful summary statistics, ancestry details, and a matched linkage-disequilibrium reference were not available.

All resources, roles, access conditions, retrieval information, and eligibility decisions are recorded in resources/data_inventory.csv and docs/data_access_and_audit.md. Discovery, orthogonal, generalization, and validation resources were kept analytically distinct. No dataset was counted as an independent validation solely because it came from a different processed file.

SCP3342 source audit and donor population

The SCP3342 portal reported 48,866 cells and 36,601 genes, with 14,644 cells annotated as cardiac muscle cell under cell_type__ontology_label. The Download page listed HFpEF_snRNAseq_single_cell_portal_10.14.2025.h5ad at approximately 3.53 GB. Portal screenshots documented a one-use, time-limited bulk-download curl command, a portal error indicating that no filename had been provided, and an interrupted transfer that reached approximately 4% before a connection reset. A subsequent retry failed because the target SCP3342/cluster/ path was not writable. These screenshots were used only for provenance and access auditing; quantitative analyses were performed from the verified local H5AD-derived products, not from screenshot values. The complete screenshot audit is provided in docs/portal_screenshot_audit.md.

The verified local H5AD source was approximately 3,795,046,162 bytes and had SHA-256 checksum 53dee7a232151ef1b296ce67a7098c8b63b44a78611311067ff74d52cad55d12. An incomplete approximately 170 MB download remnant was excluded. The H5AD contained raw_count_cellbender and raw_count_cellranger layers. Filtering cell_type__ontology_label == cardiac muscle cell yielded 14,644 cardiomyocyte nuclei from 43 donors: 19 HFpEF donors and 24 non-failing controls. Each donor contributed at least 20 cardiomyocyte nuclei, with donor-level counts ranging from 65 to 1,202. The control group included 12 female and 12 male donors; the HFpEF group included 15 female and 4 male donors. Sex and biosample/pool were included in the primary models. Nucleus counts were

used for descriptive and quality-control purposes and were not treated as independent biological replicates.

Frozen PTM-CF modules and pseudobulk processing

The PTM-CF modules were frozen before disease-effect estimation and were not selected or modified using the observed results. TLI contained 9 genes, PCI contained 15 genes, and MSI contained 15 genes. Complete definitions are provided in config/ptm_gene_modules.tsv.

Cardiomyocyte raw counts were extracted from the CellBender layer and aggregated by donor to form a gene-by-donor pseudobulk matrix. Library-size normalization and log2(CPM + 1) transformation were performed at the donor level. Module scores were calculated from donor-level normalized expression. A higher TLI represented greater translation/ribosome-associated load, a higher PCI represented greater proteostasis capacity, and a higher MSI represented greater metabolic and oxidative-phosphorylation supply.

Statistical analysis

The primary unit of inference was the donor. Treating the donor as the biological replicate is consistent with recommendations for pseudobulk analysis of single-cell data and avoids anti-conservative inference from within-donor nuclei [19,20]. Module and frozen-gene effects were estimated using donor-level normalized expression and a model of the form:

module_score ~ HFpEF + sex + biosample/pool.

For each endpoint, we report the HFpEF effect estimate β, 95% confidence interval, nominal P value, and Benjamini–Hochberg false-discovery rate (FDR). Gene-level analyses used the same donor-level design. A prespecified combination of FDR < 0.05 and absolute effect size ≥ 0.25 was used to identify high-confidence gene-level signals. Leave-one-donor-out analyses were used to assess directional stability and were not treated as independent replication.

Complete age, body-mass index, diabetes, hypertension, left-ventricular ejection fraction, medication, and other clinical covariates were not available in the H5AD metadata. The count-level workflow and multiple-testing procedures follow established RNA-sequencing analysis practice [21–23]. Accordingly, the study does not claim complete clinical confounding control. The principal model was based on CellBender donor pseudobulk counts with sex and biosample/pool adjustment.

A sensitivity PTM-CF analysis excluded prespecified ribosome-, respiratory-chain-, and ATP-synthase-related rationale groups. This sensitivity endpoint was interpreted as supportive only and did not replace the frozen primary endpoint.

Human myocardial proteomics integration

PXD045677 processed protein tables and sample annotations were audited from the public PRIDE resource. The proteomics data were treated as human myocardial tissue-level orthogonal evidence. They were not described as cardiomyocyte-specific validation because the samples were not purified cardiomyocyte proteomes.

RNA and protein measurements were matched using standardized gene symbols. We assessed directional concordance and Spearman correlation. Module-level protein evidence was calculated only when prespecified coverage gates were met. MSI coverage was 11/15 genes (73.3%) and passed the coverage gate. TLI and PCI coverage was below 70%, so complete protein-level TLI or PCI scores and a protein-derived PTM-CF score were not reported.

Mouse cross-species audit

PXD033501 represents a male mouse SAUNA-HFpEF/sham model with four animals per group. Published processed tables were re-audited for protein and phosphosite evidence using the available archived data. A limma-based

reconstruction and cyclic-loess sensitivity analysis were used. The archived reconstruction retained 2,905 proteins and 311 phosphosites after the 70% quantitative gate. It identified 830 nominally differential proteins and 69 nominally differential phosphosites; none and four, respectively, passed FDR < 0.05. Because the archived reconstruction did not fully reproduce the published counts of 897 differential proteins and 72 differential phosphosites, this resource was treated as directional generalization/sensitivity evidence rather than quantitative replication or human causal evidence.

Candidate-gene evidence audit

Candidate prioritization considered six evidence domains: (1) human cardiomyocyte transcriptional evidence; (2) at least one independent evidence layer; (3) cross-model directional consistency; (4) HFpEF specificity; (5) genetic support; and (6) tractability and safety. Because a compatible HFrEF/DCM donor-level comparator, complete genetic statistics, an independent human cardiomyocyte cohort, and intervention-safety evidence were unavailable, no candidate received a final Tier A/B/C ranking. The evidence matrix was used only to define priorities for future validation.

Immune-composition and inflammatory-state validation

A prespecified immune layer was added without changing the TLI, PCI, MSI, or PTM-CF definitions. The analysis used machine-readable `cell_type__ontology_label` annotations and donor metadata from the complete SCP3342 H5AD. Portal screenshots were not used as quantitative inputs.

We recorded macrophage, cycling-macrophage, lymphocyte, and mast-cell labels and separately retained other labels containing macrophage, lymphocyte, monocyte, dendritic, T-cell, B-cell, NK-cell, or mast-cell terms. The primary composition endpoints were the proportion of immune-labeled nuclei among all donor nuclei and the proportion represented by each immune

label. Models used the same donor-level design as the primary analysis, including phenotype, sex, and biosample/pool.

An 18-gene cardiomyocyte inflammatory module was frozen before analysis: IL1B, IL6, TNF, CCL2, CXCL8, NFKB1, RELA, NLRP3, TLR4, STAT3, JAK1, IFNG, TGFB1, ICAM1, VCAM1, HLA-DRA, HLA-DPA1, and HLA-DPB1. Cardiomyocyte CellBender counts were aggregated by donor, and an equally weighted log2(CPM + 1) score was calculated. The primary model was Inflammatory_score ~ HFpEF + sex + biosample/pool. The exploratory association model was Inflammatory_score ~ PTM_CF + sex + biosample/pool and was interpreted only as an association analysis. The module entered analysis only after the prespecified 70% gene-availability threshold was met. Immune results were not used to modify PTM-CF modules or candidate rankings.

Reproducibility and analysis gating

The project was organized with Snakemake and included resource inventories, frozen module definitions, R statistical scripts, Python validation scripts, run manifests, and figure-readiness audits. The workflow dry-run completed with no missing requested outputs. Two existing rules, immune_validation and ptmcf_sensitivity, retained missing provenance metadata from prior execution; their output files were present and were not silently treated as new analyses.

Analyses lacking eligible data were labeled NOT_RUN or BLOCKED. This applied to HFpEF-specific HFrEF/DCM interaction testing, scATAC/multiome regulatory analysis, RNA velocity, spatial co-localization, clinical-endpoint generalization, GWAS colocalization/TWAS/MR, and CMap/LINCS drug-reversal analysis.

Results

Cohort audit and evidence structure

The final evidence structure consisted of three analytically distinct layers. SCP3342 supplied the human cardiomyocyte raw-count discovery analysis. PXD045677 supplied human myocardial tissue-level proteomic evidence. PXD033501 supplied directional cross-species evidence from one small male mouse model. No compatible HFrEF/DCM cardiomyocyte donor cohort was available for a formal HFpEF-specific interaction model, and no independent human cardiomyocyte validation cohort was available.

All 43 SCP3342 donors met the prespecified cardiomyocyte-count threshold. The distribution of phenotype across biosample/pool was retained in the design matrix, and the complete H5AD was used to generate donor-level CellBender pseudobulk products. Because full clinical covariates were unavailable, the results represent a donor-level discovery analysis from a complete raw-count matrix rather than a fully clinically adjusted analysis.

TLI and MSI were lower in HFpEF cardiomyocytes

The donor-level CellBender model showed lower TLI in HFpEF, with $\beta = -0.2596$, 95% CI −0.4194 to −0.0998, and FDR = 0.00460. MSI was also lower, with $\beta = -0.2334$, 95% CI −0.3195 to −0.1472, and FDR = $1.65 \times 10-5$. These models used 43 donors as biological replicates and adjusted for sex and biosample/pool.

At the gene level, ACADVL, HADHA, and NAMPT were directionally lower within MSI; CPT1B and PPARA also showed downward trends, although not all met the prespecified effect-size threshold. DDX21 was significant within TLI but had a relatively small effect. Together, these findings support reduced metabolic/oxidative-phosphorylation and selected translation-related programs rather than cell-level significance inflation caused by treating nuclei as independent observations.

PCI was directionally lower and PTM-CF was higher in the primary model

PCI was directionally lower but not significant ($\beta = -0.0635$, 95% CI −0.1898 to 0.0628, FDR = 0.314). Under the frozen definition, the PTM-CF composite was

higher in HFpEF (β = 0.9533, 95% CI 0.1234 to 1.7832, FDR = 0.0342). This result passed the FDR threshold in the 43-donor model adjusted for sex and biosample/pool, but it remains a single-cohort finding requiring independent replication.

The result supports PTM-CF as a testable coupling model; it does not demonstrate causal proteostasis failure, therapeutic reversibility, or a disease-specific mechanism. The interpretation is further constrained by the non-significant PCI component and by the absence of an independent human cardiomyocyte cohort.

Sensitivity analysis supported but did not replace the primary endpoint

After excluding prespecified ribosome-, respiratory-chain-, and ATP-synthase-related rationale groups, the sensitivity PTM-CF effect was β = 1.090, 95% CI 0.400 to 1.779, FDR = 0.00389. Sensitivity MSI remained lower (FDR = 7.36 × 10−10), whereas TLI showed a smaller effect (FDR = 0.00389) and PCI remained non-significant (FDR = 0.992).

This result indicates that the composite may be influenced by broad mitochondrial and ribosomal gene definitions. Because it depends on the excluded-module construction, it is supportive only and does not replace the frozen primary endpoint.

RNA–protein evidence was partially concordant

In PXD045677, 25 of 39 frozen-module genes could be matched to the protein table. Seventeen of 25 genes (68%) showed concordant RNA–protein direction, but the global correlation was not significant (Spearman ρ = 0.158, P = 0.452).

ACADVL showed an RNA effect of −0.333 in human cardiomyocytes and a protein effect of −1.540 in human myocardium. HADHA showed corresponding effects of −0.318 and −2.373. COX5A showed −0.044 and −2.598, NDUFV1

showed −0.011 and −3.208, and UQCRC1 showed −0.018 and −1.342. NDUFS1, SDHA, and SQSTM1 showed RNA–protein directional discordance. The human myocardial proteome contained 335 proteins with FDR < 0.05, including 249 lower and 86 higher proteins. The tissue-level findings are considered in the context of prior human myocardial proteomic studies of HFpEF [3,24,25]. MSI protein coverage was 73.3% and passed the prespecified gate. TLI and PCI coverage was insufficient for complete protein-module scores. RNA–protein discordance was therefore treated as biologically informative but not as evidence of translation efficiency. Translation efficiency cannot be inferred without matched RNA-seq and ribosome-profiling measurements.

ACADVL and HADHA were the most convergent computational candidates

ACADVL showed lower human cardiomyocyte RNA (β = −0.333, FDR = 1.15 × 10−7), stable leave-one-donor-out direction, lower human myocardial protein (β = −1.540, protein FDR = 0.0856), and concordant mouse protein direction (β = −0.091). HADHA showed lower human cardiomyocyte RNA (β = −0.318, FDR = 4.81 × 10−6), stable leave-one-donor-out direction, lower human myocardial protein (β = −2.373, protein FDR = 0.0333), and concordant mouse protein direction (β = −0.0666).

NAMPT was directionally concordant in human cardiomyocyte RNA and human protein but not in the mouse model. LONP1 was concordant in human RNA and protein but directionally discordant in mouse. PPARA and CPT1B provided metabolic context but did not fully meet the primary candidate criteria. ACADVL and HADHA were therefore the strongest computational candidates for follow-up validation, but both remained explicitly NOT_RANKED and were not presented as validated therapeutic targets.

Mouse proteome/phosphoproteome provided limited generalization

After the 70% quantitative gate, the PXD033501 re-audit retained 2,905 proteins and 311 phosphosites. The re-analysis identified 830 nominally differential proteins and 69 nominally differential phosphosites; none and four, respectively, passed FDR < 0.05. Because the archived reconstruction did not fully reproduce the published numbers of 897 differential proteins and 72 differential phosphosites, the dataset was used only for cautious cross-species directionality and sensitivity assessment.

Immune-labeled composition changed without an overall immune-fraction increase

In the 43-donor SCP3342 analysis, the overall immune-labeled nuclear fraction did not differ significantly between HFpEF and non-failing controls (β = −0.00727, 95% CI −0.02675 to 0.01220, FDR = 0.4529). The cycling-macrophage fraction was lower in HFpEF (β = −0.00579, 95% CI −0.00856 to −0.00302, FDR = 0.000816), whereas the lymphocyte fraction was higher (β = 0.01351, 95% CI 0.00556 to 0.02146, FDR = 0.00382).

The macrophage fraction showed a nominal decrease but did not pass the FDR threshold (β = −0.01423, FDR = 0.0584). The mast-cell fraction also showed a nominal decrease but did not pass the FDR threshold (β = −0.000763, FDR = 0.0576). These findings indicate label-specific compositional differences rather than a uniform increase in immune-labeled nuclei.

Because the analysis was based on tissue single-nucleus labels, the results may be affected by sampling, nuclear capture, cell survival, and annotation uncertainty. The fractions should not be interpreted as absolute tissue cell numbers or direct measurements of immune-cell function.

Cardiomyocyte inflammatory score was not increased and was not associated with PTM-CF

The frozen 18-gene inflammatory module passed the prespecified gene-availability gate and was scored across cardiomyocytes from all 43 donors. The inflammatory score was not significantly higher in HFpEF (β = 0.110, 95% CI −0.398 to 0.619, FDR = 0.6623). The exploratory association with PTM-CF was also not significant (β = 0.152, 95% CI −0.0417 to 0.3467, FDR = 0.2395).

Thus, the immune validation supports specific immune-composition differences but does not support a generalized increase in the cardiomyocyte inflammatory module in this dataset. It also does not establish a donor-level association between the inflammatory score and PTM-CF. The null result should not be interpreted as proof that immune biology is absent. Neither the composition analysis nor the inflammatory score demonstrates immune-cell activation, cytokine release, immune–cardiomyocyte communication, or an inflammatory causal chain.

Analyses that remained not run

The available data supported figures describing study design, cohort audit, TLI/PCI/MSI/PTM-CF, immune composition, inflammatory score, RNA–protein directionality, cross-species directionality, and candidate evidence. HFpEF-specific HFrEF/DCM interaction, chromatin/TF activity, RNA velocity, spatial co-localization, clinical-endpoint generalization, GWAS colocalization/TWAS/MR, and CMap/LINCS drug-reversal analyses were not run because their prespecified data or eligibility gates were not met.

Discussion

Principal findings

This study provides two comparatively robust donor-level signals in public human HFpEF cardiomyocyte data: lower translation/ribosome-associated expression and a more pronounced reduction in metabolic/oxidative-phosphorylation expression. Both remained significant

after donor-level modeling and direction-stability auditing. PCI was directionally lower but not significant. The frozen PTM-CF composite was higher in the complete H5AD CellBender model and passed FDR < 0.05, but this remains a single-cohort result requiring independent human replication.

This interpretation is more cautious than concluding that HFpEF is proven to contain a proteostasis–translation–metabolism coupling failure. The data suggest that HFpEF cardiomyocytes may exhibit remodeling of metabolic supply and translation-related programs, while proteostasis capacity may comprise multiple opposing gene-level changes. The interpretability of the composite depends on component coherence, measurement coverage, and replication.

Metabolic remodeling as a cardiomyocyte state signal

ACADVL and HADHA participate in long-chain fatty-acid oxidation and mitochondrial fatty-acid oxidation, respectively. Their concordant direction across human cardiomyocyte RNA, human myocardial protein, and mouse HFpEF protein evidence makes them the most convergent metabolic candidates in the current audit. This pattern is consistent with broader biological models of altered substrate use and mitochondrial dysfunction in HFpEF. However, the analysis cannot determine whether these changes are causal, compensatory, markers of disease severity, or consequences of medication and comorbidity.

RNA–protein discordance is informative but not translation efficiency

Although 17/25 matched genes showed concordant direction, the global RNA–protein correlation was not significant. Protein degradation, translational control, mitochondrial import, tissue composition, and platform differences may all contribute to discordance. Concordant ACADVL and HADHA protein evidence supports further validation, but it does not establish altered

translation efficiency. Matched RNA-seq and ribosome profiling would be required to estimate translation efficiency directly.

Immune composition and cardiomyocyte inflammatory state were separable

The prespecified donor-level immune analysis found a higher lymphocyte fraction and lower cycling-macrophage fraction in HFpEF, without a significant change in the overall immune-labeled fraction. This interpretation is consistent with experimental evidence that myeloid populations can shape hypertensive heart-failure remodeling, while remaining distinct from proof of immune activation in the present dataset [26,27,29]. This pattern suggests label-specific composition remodeling rather than global immune expansion. The tissue single-nucleus design limits interpretation of absolute cell abundance and functional activation.

The cardiomyocyte inflammatory score was not significantly higher in HFpEF and was not associated with PTM-CF. In the current data, immune composition and cardiomyocyte metabolic/proteostasis remodeling should therefore be treated as parallel, not causally connected, observations. Direct cytokine measurements, independent human immune validation, ligand–receptor evidence, and functional immune–cardiomyocyte assays remain necessary.

Boundaries for candidate and therapeutic interpretation

ACADVL and HADHA are computationally convergent candidates, but they lack HFpEF-versus-HFrEF/DCM specificity testing, complete clinical adjustment, independent human cardiomyocyte replication, genetic directionality, and tissue-selective intervention-safety evidence. NAMPT and LONP1 show human RNA–protein concordance but unstable cross-model direction. The study therefore nominates candidates for experimental prioritization and does not claim that any candidate restores myocardial function or has therapeutic efficacy.

Limitations

1. **Incomplete clinical covariates.** Age, body-mass index, diabetes, hypertension, left-ventricular ejection fraction, medications, and other clinical variables were not available in the H5AD metadata. The model adjusted sex and biosample/pool but did not provide complete clinical confounding control.
2. **Single human discovery cohort.** The PTM-CF result was obtained in one human cohort and requires independent replication.
3. **HFpEF specificity was not tested.** No compatible HFrEF/DCM donor-level cardiomyocyte comparator was available for the prespecified interaction analysis.
4. **No independent human cardiomyocyte validation cohort.** Mouse datasets cannot substitute for independent human validation.
5. **Human proteomics was tissue-level.** PXD045677 was not a purified cardiomyocyte proteome, and TLI/PCI protein coverage was insufficient for complete module scoring.
6. **Mouse sample size and reconstruction differences.** PXD033501 included four male mice per group and the archived reconstruction did not fully reproduce the published differential-feature counts.
7. **Genetic and drug analyses were not run.** Complete ni-HFpEF GWAS statistics, matched linkage disequilibrium, and eligible drug-perturbation evidence were not available under the prespecified gates.
8. **Immune interpretation is limited.** Single-nucleus labels cannot directly establish absolute cell numbers, activation state, cytokine release, or cell–cell communication. The inflammatory score was not significantly altered or associated with PTM-CF.
9. **Observational design.** All results are associative and cannot establish causality or predict response to intervention.

Conclusion

In a complete H5AD raw-count analysis, HFpEF cardiomyocytes showed stable reductions in translation-related and metabolic/oxidative-phosphorylation expression, particularly in fatty-acid oxidation and mitochondrial programs. PCI was directionally lower but not significant, whereas the frozen PTM-CF composite passed FDR < 0.05 in the sex- and biosample/pool-adjusted donor model. The additional donor-level immune analysis found a higher lymphocyte fraction and lower cycling-macrophage fraction without a significant increase in the overall immune-labeled fraction. The cardiomyocyte inflammatory score was neither significantly higher nor significantly associated with PTM-CF.

These findings provide an auditable immune-related validation layer but do not establish immune activation, inflammatory causality, immune–cardiomyocyte communication, HFpEF specificity, therapeutic efficacy, or target validation. ACADVL and HADHA are computationally convergent candidates for follow-up experiments but remain NOT_RANKED. Priority next steps are compatible HFrEF/DCM comparison, independent human cardiomyocyte and immune validation, protein/cytokine and communication assays, and cardiomyocyte-specific testing of mitochondrial fatty-acid oxidation and proteostasis mechanisms.

Data availability statement

The study used publicly available resources. Human single-nucleus discovery data were obtained from Broad Single Cell Portal SCP3342; human myocardial proteomics were obtained from PRIDE/ProteomeXchange accession PXD045677; and mouse HFpEF proteome/phosphoproteome data were obtained from PRIDE accession PXD033501. Resource URLs, roles, access status, retrieval information, and eligibility decisions are documented in resources/data_inventory.csv and docs/data_access_and_audit.md.

The complete SCP3342 H5AD source used for the primary CellBender analysis is retained locally under the applicable portal terms. Its SHA-256

checksum is recorded in the run manifest and audit documentation. Restricted or repository-controlled source files are not redistributed.

Code availability statement

The Snakemake workflow, frozen PTM-CF module definitions, R and Python analysis scripts, metadata validation, public-data audit scripts, figure-generation scripts, analysis-gate summaries, run manifests, and figure-readiness ledger are included in the project package.

Ethics statement

This study used publicly available, de-identified datasets and did not recruit new human participants or conduct new animal experiments. The authors should confirm whether the target journal requires an additional institutional-exemption statement or accession-specific ethics wording.

Funding

This work was supported by the Capacity Enhancement Grant for the Supervisor Team of the the Stomatology Key Program of Southwest Medical University in 2024 (No. 2024KQZX01)，School of Stomatology of Southwest Medical University (No. 2025DS08), and the Innovative Leading Talents Program of the Affiliated Stomatological Hospital of Southwest Medical University (No. 2022LJ02).

Conflict of interest

The authors declare that the research was conducted in the absence of any commercial.

Author contributions

C Z and X L designed and directed the study, provided funding support for the study, wrote the final version of the manuscript, and is the PI of this study. Y H and H T wrote the manuscript, R P and J M reviewed and revised the manuscript. H Z performed visualization, All authors read and approved the final version of the manuscript.

Acknowledgments

Not applicable.

Clinical trial registration

Clinical trial number: not applicable.

Figure legends

Figure 1. Human-first, donor-level, non-leaky study design. The figure should show the SCP3342 human cardiomyocyte discovery layer, PXD045677 human myocardial proteomics orthogonal layer, PXD033501 mouse generalization layer, and genetics/drug layers that remained gated. Each layer should display tissue, species, sample role, and access limitations.

Figure 2. Donor and cardiomyocyte-nucleus overview of the SCP3342 discovery cohort. The figure should show 43 donors, including 19 HFpEF and 24 non-failing controls, together with the number of cardiomyocyte nuclei per donor. Nucleus counts are presented for quality and descriptive auditing and are not treated as independent biological replicates.

Figure 3. Translation, proteostasis, metabolism, and PTM-CF module results. Show donor-level points, adjusted HFpEF effects, 95% confidence intervals, and FDR for TLI, PCI, MSI, and PTM-CF. TLI and MSI are lower, PCI is directionally lower but not significant, and the frozen PTM-CF composite is higher in the complete H5AD CellBender model. The figure should distinguish the primary complete-H5AD model from anonymous-API sensitivity analyses.

Figure 4. Donor-level immune-labeled composition. Show overall immune-labeled fraction and the fractions of lymphocytes, cycling macrophages, macrophages, and mast cells, with donor-level observations, adjusted effects, and 95% confidence intervals. Highlight the higher lymphocyte fraction and lower cycling-macrophage fraction while noting that the overall immune-labeled fraction was not significantly different.

Figure 5. Cardiomyocyte inflammatory-score validation. Show the 18-gene module availability, HFpEF effect, and exploratory association with

PTM-CF. Neither endpoint is FDR-significant. The figure should state that these results do not establish absence of immune biology or causality.

Figure 6. Human cardiomyocyte RNA–human myocardial protein directional concordance. Show RNA effects against protein effects for 25 matched frozen-module genes, with concordant and discordant quadrants. Report 17/25 concordant directions and Spearman $\rho = 0.158$, $P = 0.452$. The figure should identify the tissue-level nature of the protein evidence.

Figure 7. Cross-species protein and phosphosite audit. Show retained feature counts, nominally differential counts, and FDR-gated counts for PXD033501. Emphasize that this is small-sample sensitivity/generalization evidence, not quantitative replication.

Figure 8. Candidate evidence matrix. Show ACADVL, HADHA, NAMPT, LONP1, PPARA, and CPT1B across human cardiomyocyte RNA, human myocardial protein, mouse protein, specificity, genetics, and safety domains. ACADVL and HADHA have the strongest current convergence, but all candidates remain NOT_RANKED.

Supplementary materials

Supplementary Table 1. Data resources, access status, and analytical roles.

Supplementary Table 2. Donor inclusion, sex, biosample/pool, and cardiomyocyte-nucleus counts.

Supplementary Table 3. Complete gene-level effects for the 39 frozen-module genes.

Supplementary Table 4. Module coverage, module scores, and sensitivity analyses.

Supplementary Table 5. PXD045677 RNA–protein matching and missingness audit.

Supplementary Table 6. PXD033501 protein/phosphosite audit and sensitivity reconstruction.

Supplementary Table 7. Candidate evidence matrix and unmet advancement

gates.

Supplementary Table 8. Run manifest, software versions, source-file checksums, and figure-readiness audit.

Supplementary Figure 1. SCP3342 portal and download provenance audit screenshots. Screenshots are provenance evidence only and are not quantitative analysis inputs.

References

1. Broad Institute Single Cell Portal. Single cell transcriptomic analyses of human heart failure with preserved ejection fraction. Study SCP3342 [Internet]. Available from: https://singlecell.broadinstitute.org/single_cell/study/SCP3342/single-cell-transcriptomic-analyses-of-human-heart-failure-with-preserved-ejection-fraction. Accessed 2026 Sep 22.

2. ProteomeXchange Consortium. Human myocardial proteomics dataset PXD045677 [Internet]. Available from: https://www.ebi.ac.uk/pride/archive/projects/PXD045677. Accessed 2026 Sep 22.

3. Valero-Muñoz M, Saw EL, Hekman RM, Blum BC, Hourani Z, Granzier H, et al. Proteomic and phosphoproteomic profiling in heart failure with preserved ejection fraction (HFpEF). Front Cardiovasc Med. 2022;9:966968. doi:10.3389/fcvm.2022.966968.

4. ProteomeXchange Consortium. Mouse SAUNA-HFpEF proteome/phosphoproteome dataset PXD033501 [Internet]. Available from: https://www.ebi.ac.uk/pride/archive/projects/PXD033501. Accessed 2026 Sep 22.

5. HERMES investigators. Genetic architecture of non-ischemic heart failure with preserved ejection fraction. Nat Genet. 2024. doi:10.1038/s41588-024-02064-3.

6. Heart Cell Atlas Consortium. Human Heart Cell Atlas [Internet]. Available from: https://www.heartcellatlas.org/. Accessed 2026 Sep 22.

7. Borlaug BA. The pathophysiology of heart failure with preserved ejection fraction. Nat Rev Cardiol. 2014;11:507-515. doi:10.1038/nrcardio.2014.83.

8. Paulus WJ, Tschöpe C. A novel paradigm for heart failure with preserved ejection fraction. J Am Coll Cardiol. 2013;62:263-271. doi:10.1016/j.jacc.2013.02.092.

9. Shah SJ, Kitzman DW, Borlaug BA, et al. Phenotype-specific treatment of heart failure with preserved ejection fraction. Circulation. 2016;134:73-90. doi:10.1161/CIRCULATIONAHA.116.021884.

10. Shah SJ, Lam CSP, Svedbo F, et al. Prevalence and correlates of coronary microvascular dysfunction in heart failure with preserved ejection fraction. Eur J Heart Fail. 2018;20:1194-1202. doi:10.1002/ejhf.1190.

11. Dunlay SM, Roger VL, Redfield MM. Epidemiology of heart failure with preserved ejection fraction. Nat Rev Cardiol. 2017;14:591-602. doi:10.1038/nrcardio.2017.65.

12. Paulus WJ, Tschope C. A novel paradigm for heart failure with preserved ejection fraction. J Am Coll Cardiol. 2013;62:263-271. doi:10.1016/j.jacc.2013.02.092.

13. Franssen C, Chen S, Unger A, et al. Myocardial microvascular inflammatory endothelial activation in heart failure with preserved ejection fraction. JACC Heart Fail. 2016;4:312-324. doi:10.1016/j.jchf.2015.10.007.

14. Gevaert AB, Boen JR, Segers VFM, Van Craenenbroeck EM. The role of endothelial dysfunction in the pathophysiology of heart failure with preserved ejection fraction. Cardiovasc Res. 2017;113:1538-1550. doi:10.1093/cvr/cvx154.

15. Taegtmeyer H, Sen S, Vela D. Return to the fetal gene program: a suggested

679 metabolic link to gene expression in the heart. Ann N Y Acad Sci. 2010;1188:191-198.
680 doi:10.1111/j.1749-6632.2009.05100.x.
681
682 16. Bertero E, Maack C. Metabolic remodelling in heart failure. Cardiovasc Res.
683 2018;114:1305-1320. doi:10.1093/cvr/cvy061.
684
685 17. van Bilsen M, van der Vusse GJ, Reneman RS. Transcriptional regulation of
686 contractile protein gene expression in cardiac hypertrophy. Cardiovasc Res.
687 1996;31:443-450.
688
689 18. Willis MS, Patterson C. Proteotoxicity and cardiac dysfunction—Alzheimer's disease
690 of the heart? N Engl J Med. 2013;368:455-464. doi:10.1056/NEJMra1106185.
691
692 19. Crowell HL, Soneson C, Germain PL, et al. Muscat detects subpopulation-specific
693 state transitions from multi-sample multi-condition single-cell transcriptomics data. Nat
694 Commun. 2020;11:6077. doi:10.1038/s41467-020-19894-4.
695
696 20. Squair JW, Gautier M, Kathe C, et al. Confronting false discoveries in single-cell
697 differential expression. Nat Commun. 2021;12:5692. doi:10.1038/s41467-021-25960-2.
698
699 21. Robinson MD, McCarthy DJ, Smyth GK. edgeR: a Bioconductor package for
700 differential expression analysis of digital gene expression data. Bioinformatics.
701 2010;26:139-140. doi:10.1093/bioinformatics/btp616.
702
703 22. Ritchie ME, Phipson B, Wu D, et al. limma powers differential expression analyses for
704 RNA-sequencing and microarray studies. Nucleic Acids Res. 2015;43:e47.
705 doi:10.1093/nar/gkv007.
706
707 23. Benjamini Y, Hochberg Y. Controlling the false discovery rate: a practical and powerful
708 approach to multiple testing. J R Stat Soc Series B. 1995;57:289-300.

709 doi:10.1111/j.2517-6161.1995.tb02031.x.
710
711 24. Jani VP, Yoo EJ, Binek A, et al. Myocardial proteome in human heart failure with
712 preserved ejection fraction. J Am Heart Assoc. 2025;14:e038945.
713 doi:10.1161/JAHA.124.038945.
714
715 25. Hahn VS, Chaffin M, Simonson B, et al. Single cell analysis of human heart failure with
716 preserved ejection fraction. Circ Res. 2026;139:e327433.
717 doi:10.1161/CIRCRESAHA.125.327433.
718
719 26. Smart CD, Fehrenbach DJ, Wassenaar JW, et al. Immune profiling of murine cardiac
720 leukocytes identifies triggering receptor expressed on myeloid cells 2 as a novel mediator
721 of hypertensive heart failure. Cardiovasc Res. 2023;119:2312-2328.
722 doi:10.1093/cvr/cvad093.
723
724 27. Hulsmans M, Sager HB, Roh JD, et al. Cardiac macrophages promote diastolic
725 dysfunction. J Exp Med. 2018;215:423-440. doi:10.1084/jem.20171278.
726
727 28. Epelman S, Lavine KJ, Randolph GJ. Origin and functions of tissue macrophages.
728 Immunity. 2014;41:21-35. doi:10.1016/j.immuni.2014.06.013.
729
730 29. Frangogiannis NG. The inflammatory response in myocardial injury, repair, and
731 remodelling. Nat Rev Cardiol. 2014;11:255-265. doi:10.1038/nrcardio.2014.28.
732
733 30. Swirski FK, Nahrendorf M. Leukocyte behavior in atherosclerosis, myocardial
734 infarction, and heart failure. Science. 2013;339:161-166. doi:10.1126/science.1230719.
735
736 31. McMurray JJV, Solomon SD, Inzucchi SE, et al. Dapagliflozin in patients with heart
737 failure and reduced ejection fraction. N Engl J Med. 2019;381:1995-2008.
738 doi:10.1056/NEJMoa1911303.

32. Anker SD, Butler J, Filippatos G, et al. Empagliflozin in heart failure with a preserved ejection fraction. N Engl J Med. 2021;385:1451-1461. doi:10.1056/NEJMoa2107038.

33. Solomon SD, McMurray JJV, Claggett B, et al. Dapagliflozin in heart failure with mildly reduced or preserved ejection fraction. N Engl J Med. 2022;387:1089-1098. doi:10.1056/NEJMoa2206286.

34. Pitt B, Pfeffer MA, Assmann SF, et al. Spironolactone for heart failure with preserved ejection fraction. N Engl J Med. 2014;370:1383-1392. doi:10.1056/NEJMoa1313731.

35. Solomon SD, McMurray JJV, Anand IS, et al. Angiotensin-neprilysin inhibition in heart failure with preserved ejection fraction. N Engl J Med. 2019;381:1609-1620. doi:10.1056/NEJMoa1908655.

36. Heidenreich PA, Bozkurt B, Aguilar D, et al. 2022 AHA/ACC/HFSA guideline for the management of heart failure. Circulation. 2022;145:e895-e1032. doi:10.1161/CIR.0000000000001063.

37. Zheng Z, Ma C, Zhang X, et al. Single-cell transcriptomic profiling reveals cell type heterogeneity between HFpEF and HFrEF. Commun Biol. 2025;8. doi:10.1038/s42003-025-08827-w.

38. Butler J, Fonarow GC, Zile MR, et al. Developing therapies for heart failure with preserved ejection fraction: current state and future directions. JACC Heart Fail. 2014;2:97-112. doi:10.1016/j.jchf.2013.10.006.

39. Redfield MM, Borlaug BA. Heart failure with preserved ejection fraction: a review. JAMA. 2023;329:827-838. doi:10.1001/jama.2023.0241.

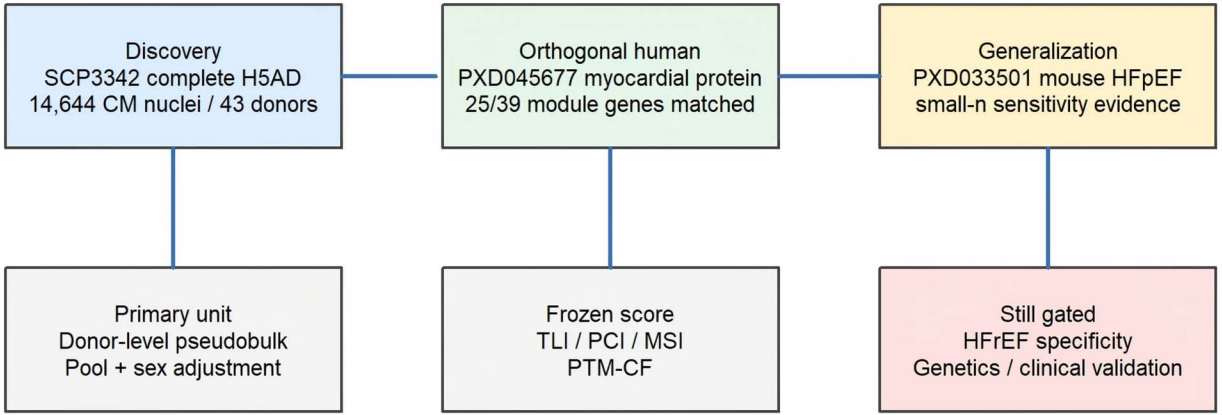
769 40. Shah AM, Shah SJ. Current approaches to the diagnosis and management of heart
770 failure with preserved ejection fraction. Circulation. 2017;136:1190-1208.
771 doi:10.1161/CIRCULATIONAHA.117.030250.
772
773 41. Dick SA, Epelman S. Chronic heart failure and inflammation: what do we really know?
774 Circ Res. 2016;119:159-176. doi:10.1161/CIRCRESAHA.116.308030.
775
776 42. Lam CSP, Donal E, Kraigher-Krainer E, Vasan RS. Epidemiology and clinical course
777 of heart failure with preserved ejection fraction. Eur J Heart Fail. 2011;13:18-28.
778 doi:10.1093/eurjhf/hfq121.
779
780 43. Maron BA, Barsten SL, Lei C, et al. Pulmonary hypertension associated with left heart
781 disease: evolving concepts and emerging mechanisms. Circulation. 2018;137:176-197.
782 doi:10.1161/CIRCULATIONAHA.117.031748.
783
784 44. Owan TE, Hodge DO, Herges RM, Jacobsen SJ, Roger VL, Redfield MM. Trends in
785 prevalence and outcome of heart failure with preserved ejection fraction. N Engl J Med.
786 2006;355:251-259. doi:10.1056/NEJMoa052256.
787
788 45. Shah SJ, Katz DH, Selvaraj S, et al. Phenomapping for novel classification of heart
789 failure with preserved ejection fraction. Circulation. 2015;131:269-279.
790 doi:10.1161/CIRCULATIONAHA.114.010637.
791
792 46. Seferovic PM, Paulus WJ. Clinical diabetic cardiomyopathy: a two-faced disease with
793 restrictive and dilated phenotypes. Eur Heart J. 2015;36:1718-1727.
794 doi:10.1093/eurheartj/ehv134.
795
796 47. Reddy YNV, Carter RE, Obokata M, Redfield MM, Borlaug BA. A simple,
797 evidence-based approach to help guide diagnosis of heart failure with preserved ejection
798 fraction. Circulation. 2018;138:861-870. doi:10.1161/CIRCULATIONAHA.118.034646.

48. Sharma K, Kass DA. Heart failure with preserved ejection fraction: mechanisms, clinical features, and therapies. Circ Res. 2014;115:79-96. doi:10.1161/CIRCRESAHA.115.302922.

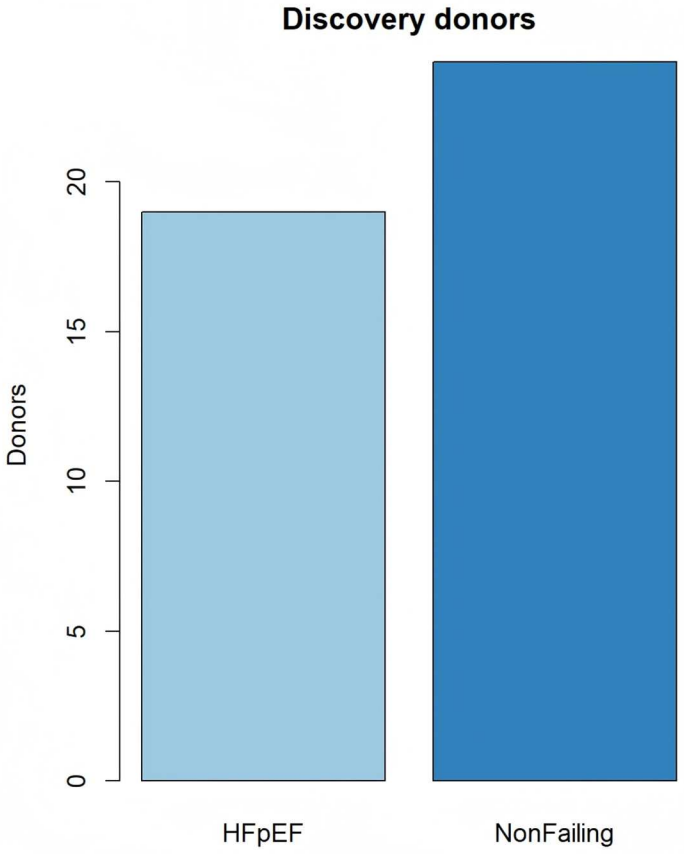
49. Zile MR, Baicu CF, Ikonomidis JS, et al. Myocardial stiffness in patients with heart failure and a preserved ejection fraction. Circulation. 2015;131:1247-1259. doi:10.1161/CIRCULATIONAHA.114.013215.

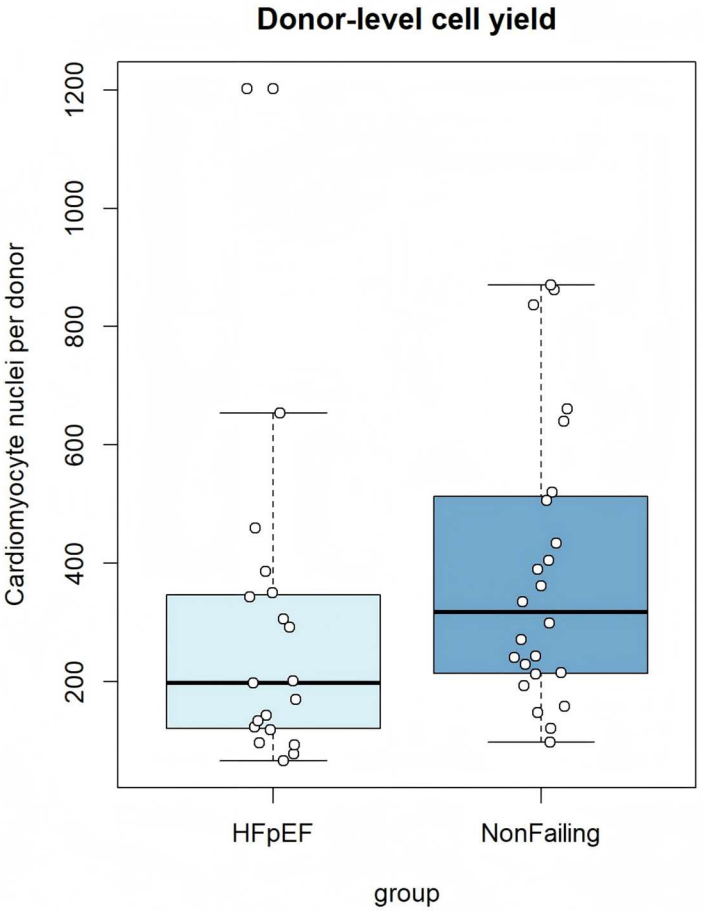
50. Simmonds SJ, Cuijvers I, Heymans S, Jones EAV. Cellular and molecular differences between HFpEF and HFrEF: a step ahead in the understanding of the pathophysiology. Nat Rev Cardiol. 2020;17:705-722. doi:10.1038/s41569-020-0355-0.

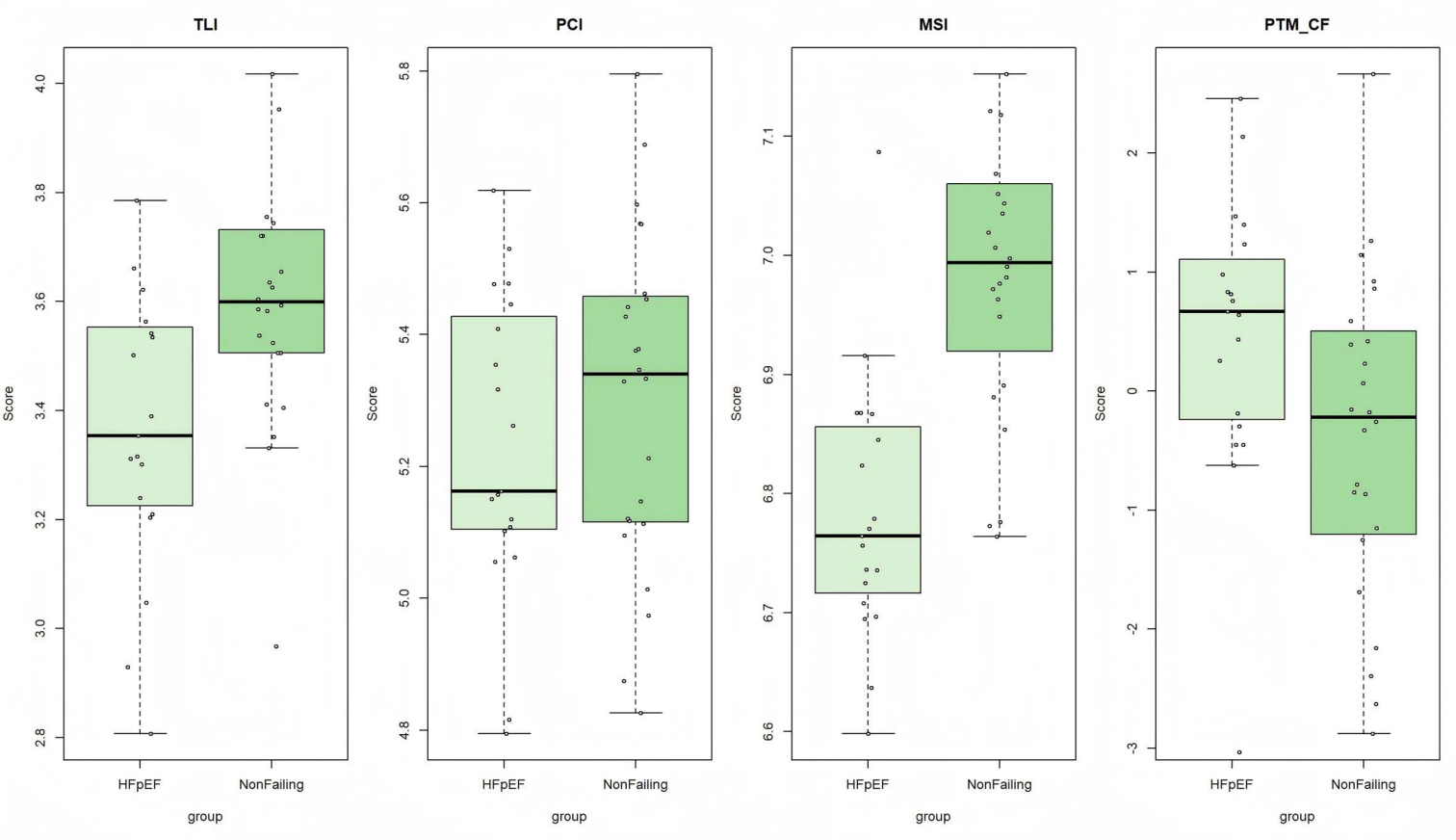
HFpEF PTM-CF study design — current audited state

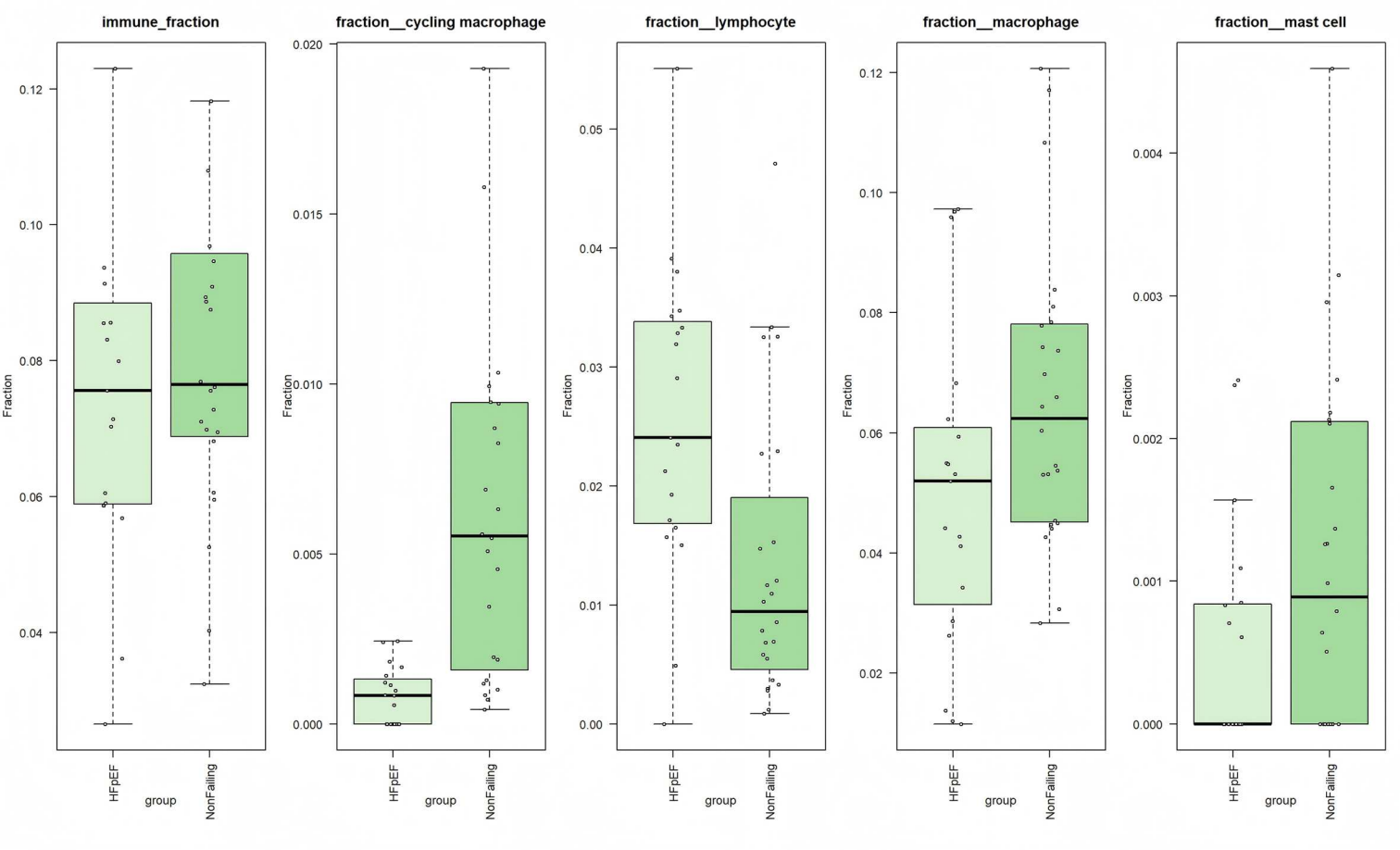


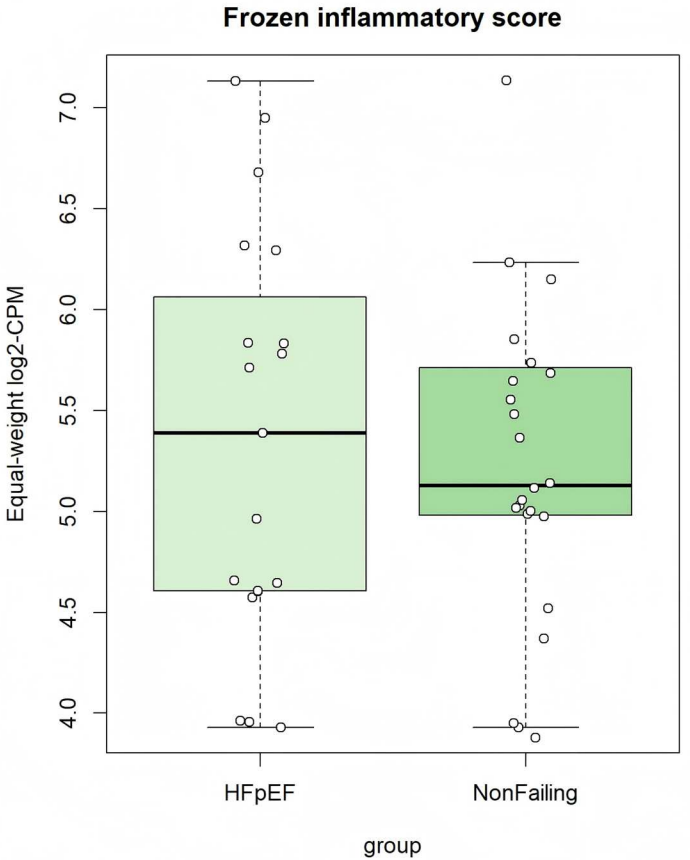
Interpretation: discovery and orthogonal evidence are available; specificity, causality and treatment claims remain blocked.

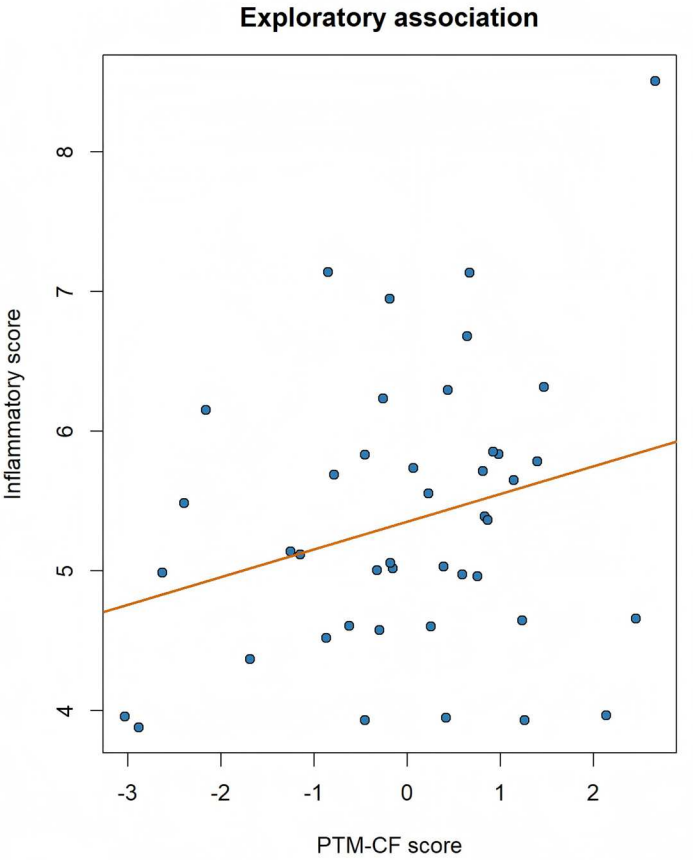

Discovery donors
Donors
0
5
10
15
20
HFpEF
NonFailing

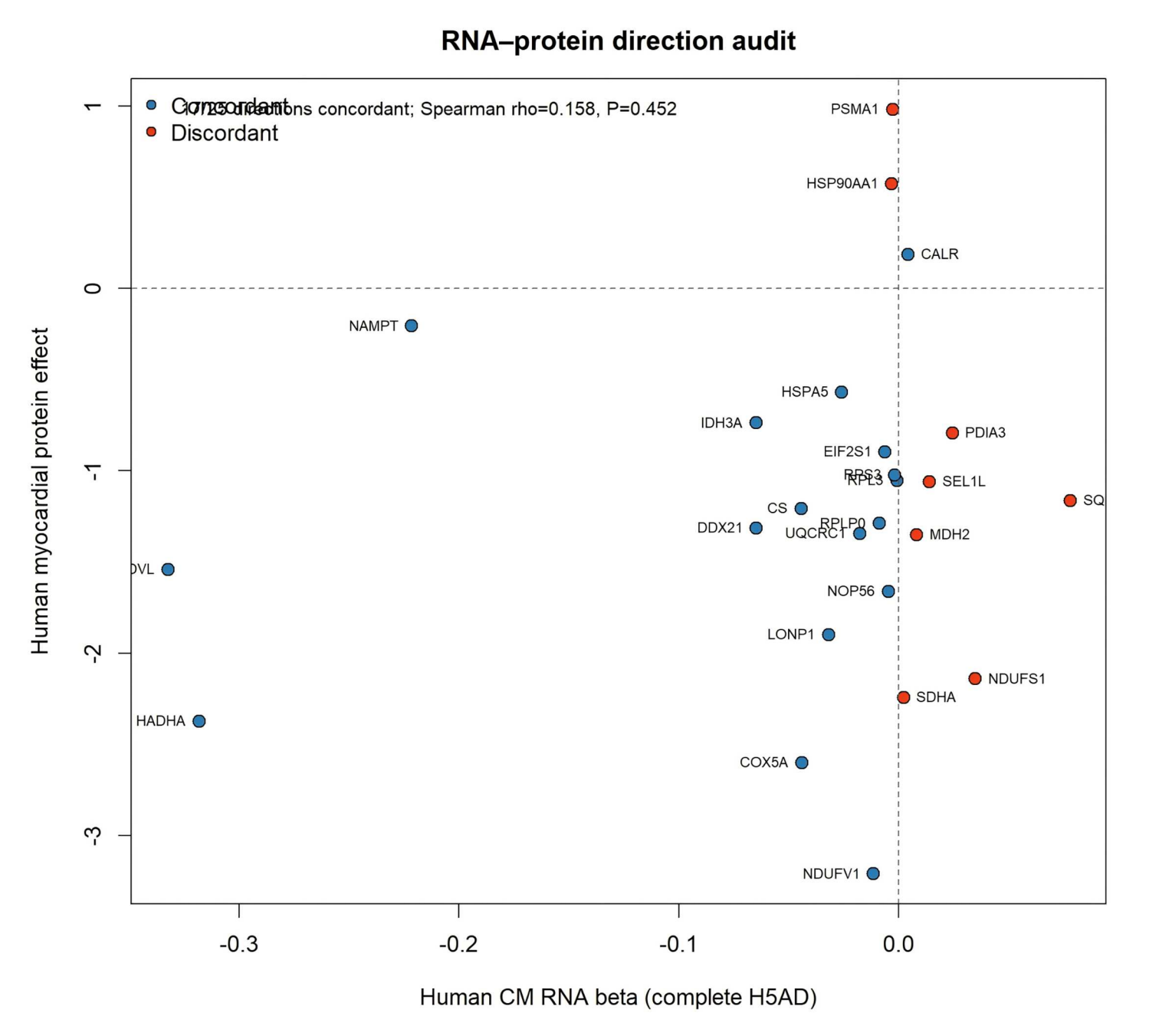

Donor-level cell yield
Cardiomyocyte nuclei per donor
200
400
600
800
1000
1200
HFpEF
NonFailing
group

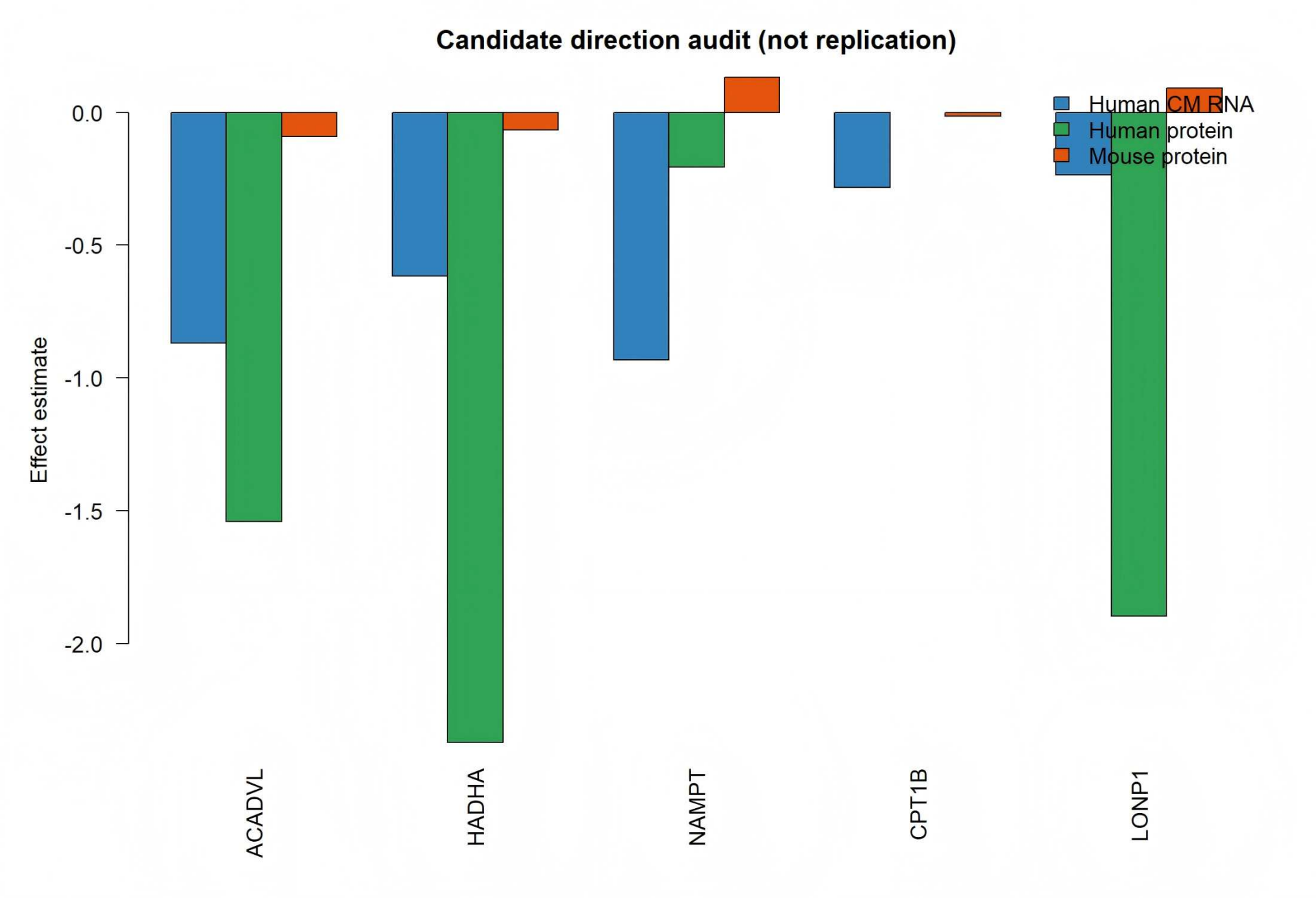

TLI
PCI
MSI
PTM_CF
Score
group
HFpEF
NonFailing
4.0
3.8
3.6
3.4
3.2
3.0
2.8
5.8
5.6
5.4
5.2
5.0
4.8
7.1
7.0
6.9
6.8
6.7
6.6
2
1
0
-1
-2
-3

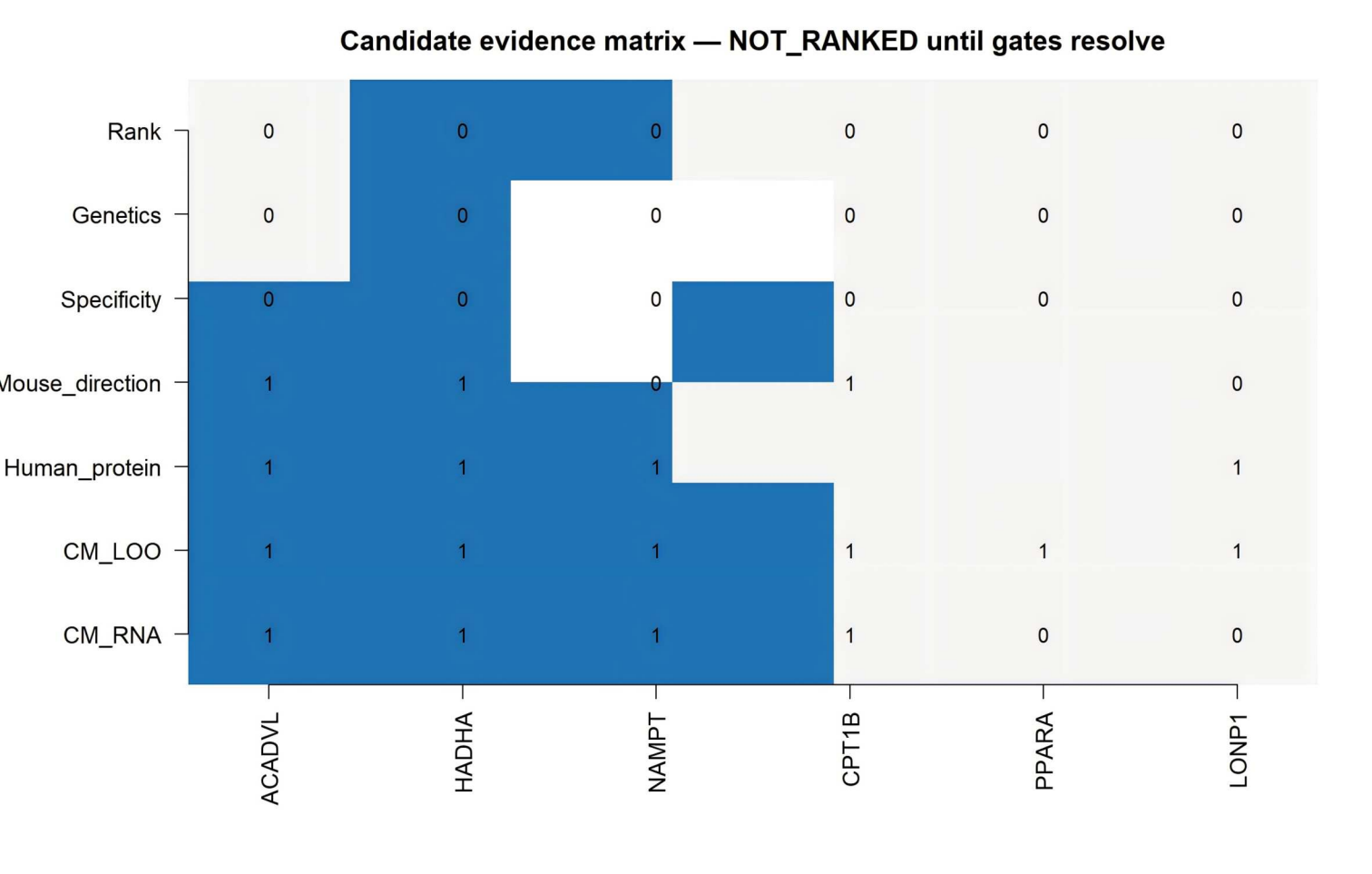

immune_fraction
fraction__cycling macrophage
fraction__lymphocyte
fraction__macrophage
fraction__mast cell
Fraction
group
HFpEF
NonFailing


Frozen inflammatory score
Equal-weight log2-CPM
4.0
4.5
5.0
5.5
6.0
6.5
7.0
HFpEF
NonFailing
group


Exploratory association
Inflammatory score
4
5
6
7
8
-3
-2
-1
0
1
2
PTM-CF score


RNA–protein direction audit
Concordant
Discordant
17/25 directions concordant; Spearman rho=0.158, P=0.452
PSMA1
HSP90AA1
CALR
NAMPT
HSPA5
IDH3A
PDIA3
EIF2S1
RPS3
RPL3
SEL1L
SQ
CS
DDX21
RPLP0
UQCRC1
MDH2
NOP56
LONP1
NDUFS1
SDHA
HADHA
COX5A
NDUFV1
Human myocardial protein effect
Human CM RNA beta (complete H5AD)
1
0
-1
-2
-3
-0.3
-0.2
-0.1
0.0


Candidate direction audit (not replication)
Effect estimate
0.0
-0.5
-1.0
-1.5
-2.0
Human CM RNA
Human protein
Mouse protein
ACADVL
HADHA
NAMPT
CPT1B
LONP1


Candidate evidence matrix — NOT_RANKED until gates resolve
Rank
Genetics
Specificity
Mouse_direction
Human_protein
CM_LOO
CM_RNA
0 0 0 0 0 0
0 0 0 0 0 0
0 0 0 0 0 0
1 1 0 1 0
1 1 1 1
1 1 1 1 1 1
1 1 1 1 0 0
ACADVL
HADHA
NAMPT
CPT1B
PPARA
LONP1

Supplementary Files

This is a list of supplementary files associated with this preprint. Click to download.

- SupplementaryTablesS1S10merged.xlsx
- CodeManifestandReproducibilityRecord.docx